Research Square

Preprints are preliminary reports that have not undergone peer review.
They should not be considered conclusive, used to inform clinical practice,
or referenced by the media as validated information.

Assessment and Modeling of Air Gap Membrane Distillation Unit

Mohamed H. Koura

Mohamed.kora@hti.edu.eg

Higher Technological Institute, Tenth of Ramadan City

M. G. Mousa

Damietta University

Mohamed Khairat Dawood

Damanhour University

Tamer Nabil

Suez Canal University

Khaled Ramzy

Suez Canal University

Research Article

Keywords: AGMD, Distillation, Thermal Efficiency- Modeling, GOR, Optimization

Posted Date: October 30th, 2026

DOI: https://doi.org/10.21203/rs.3.rs-11268618/v1

License: This work is licensed under a Creative Commons Attribution 4.0 International License.
Read Full License

Additional Declarations: No competing interests reported.

Assessment and Modeling of Air Gap Membrane Distillation Unit

Mohamed H. Koura [1, 4*], M. G. Mousa [2], Mohamed Khairat Dawood [3], Tamer Nabil [4], Khaled Ramzy[4]

1 Mechanical Department, Higher Technological Institute, Tenth of Ramadan City, Egypt, email: Mohamed.kora@hti.edu.eg
2 Mechanical Department, Faculty of Engineering, Damietta University, New Damietta City, Egypt, email: Mgmousa@du.edu.eg
3 Mechanical Power Department, Faculty of Engineering, Damanhour University, Damanhour City, Egypt, email: Mohamed.Dawood@eng.dmu.edu.eg
4 Mechanical Power Department, Faculty of Engineering, Suez Canal University, Ismailia City, Egypt, email: Tamir.Nabil@eng.suez.edu.eg, Kh.ramzy2005@eng.suez.edu.eg
* *Mohamed H Koura, Email address: Mohamed.kora@hti.edu.eg*

Abstract

This research presents an extensive thermodynamic and transport model for an Air Gap Membrane Distillation (AGMD) system, aimed at assessing thermal efficiency. This research presents an extensive thermodynamic and transport model for an (AGMD) system, aimed at assessing thermal efficiency. under varying operational conditions. The MATLAB-implemented model incorporates essential heat and mass transfer processes, such as Knudsen-molecular diffusion and conductive heat losses, to calculate key performance metrics like permeate flux, thermal efficiency, (GOR), and (STEC). The AGMD configuration utilizes a hydrophobic polytetrafluoroethylene (PTFE) membrane featuring a 5 mm air gap, a pore dimension of 0.45 μm and a surface thickness of 150 μm. Experimental simulations investigate operational parameters, with feed temperatures varying from 40°C to 70°C and coolant temperatures fluctuating between 10°C and 25°C. Research demonstrates that elevating the feed temperature improves system efficiency, resulting in a peak permeate flow rate of 12.77 kg/m²·h, a thermal efficiency of 50.62%, and a minimum (STEC) of 29.04 kWh/m³ at a feed temperature of 70°C and a coolant temperature of 10°C. These results highlight AGMD's potential as an energy-efficient desalination method, supporting sustainable freshwater generation in regions facing water scarcity. Future studies could explore optimizing membrane materials, minimizing thermal losses, and coupling with renewable energy to enhance performance and scalability. The model's accuracy is validated by a ~60% increase in GOR, closely matching experimental outcomes. A custom built, solar integrated AGMD test rig equipped with a flat-plate solar collector and Arduino-based real-time monitoring was used to verify the model. Predictions showed strong alignment with experimental data and existing literature, confirming the system's scalability and robustness. With an advantageous freshwater production expense of $2.52 per cubic meter, the system emerges as a practical solution for decentralized, off-grid applications. This research establishes a validated MATLAB modeling framework to guide AGMD design optimization, promoting its adoption as an affordable, renewable energy-powered desalination technology.

Keywords: AGMD – Distillation – Thermal Efficiency- Modeling – GOR – Optimization.

Nomenclature

Symbol	Unit	Description
A	[m²]	Membrane surface area
$C_{p,f}$	[J/kg·K]	Specific heat capacity of feed water
D	[m²/s]	Diffusion coefficient
d_p	[μm]	Pore diameter
F_d	[L/h]	Flow rate of distilled water
F_f	[L/h]	Inlet water flow rate
J / Jp	[kg/m²·h]	Permeate flux
km	[W/m·K]	Membrane's thermal conductivity
κ_a	[W/m·K]	The thermal conductivity of atmospheric air
M	[Pa·s]	Dynamic viscosity
$\dot{m}$	[kg/s]	Mass flow rate
P	[USD]	Capital cost
P_n	[m³/year]	Annual water production
ρ_f	[kg/m³]	Feed water density
ρ_d	[kg/m³]	Distillate water density
Q	[W]	Thermal energy
Rm	[s/m]	Membrane resistance
R_a	[s/m]	Air gap resistance
R	[–]	Rayleigh number
ΔH	[J/kg]	Latent heat of evaporation
Δt	[h]	Sampling time
STEC	[kWh/m³]	Specific thermal energy consumption

TE	[%]	Thermal efficiency
$T_{f,in}$	[°C]	Inlet feed temperature
$T_{f,out}$	[°C]	Outlet feed temperature
$T_{p,in}$	[°C]	Permeate inlet temperature
$T_{p,out}$	[°C]	Permeate outlet temperature
i	[%]	Annual rate of interest
n	[year]	Lifetime years

Abbreviations

Acronym	Meaning
AGMD	Air Gap Membrane Distillation
AMC	Annual Maintenance Cost
ASV	Annual Salvage Value
CPL	Cost Per Liter
CRF	Capital Recovery Factor
DC	Direct Current
DCMD	Direct Contact Membrane Distillation
ED	Electrodialysis
FAC	First Annual Cost
FPC	Flat Plate Collector
GOR	Gained Output Ratio
MD	Membrane Distillation
MED	Multiple Effect Distillation
MPC	Model Predictive Controller
MSF	Multiple Stage Flash
Ppm	Parts Per Million
PTFE	Polytetrafluoroethylene
PV	Photovoltaic
RO	Reverse Osmosis
SGMD	Sweeping Gas Membrane Distillation
SFF / SSF	Sinking Fund Factor
SMDDS	Solar Membrane Distillation Desalination System
TE	Thermal Efficiency
UV	Ultraviolet
VMD	Vacuum Membrane Distillation

Greek Symbols

Symbol	Unit	Description
ε	[–]	Membrane porosity
τ	[–]	Membrane tortuosity
β	[1/K]	Coefficient of thermal expansion
ν	[m²/s]	Air kinematic viscosity
η	[%]	Efficiency
α	[m²/s]	Air thermal diffusivity
Σ	[N/m]	Surface tension
Δ	[m]	Membrane thickness
Π	[Pa]	Osmotic pressure

1. Introduction

Scientists have been diligently pursuing the most prevalent and efficient techniques for generating potable water to enhance both the volume and quality of clean water. Water is a common chemical substance composed of hydrogen and oxygen atoms. It is a common, tasteless, and transparent material present on the Earth's exterior. Water manifests in three forms: solid, liquid, and gaseous. Its condition alters in response to temperature. Roughly 70% of the Earth's expanse is enveloped by water, totaling 1.4×10^9 km³ (U.S. Geological, 2023). Out of all the Earth's water, 97% is saline, 1% is potable freshwater, and 2% is confined in polar ice. (The Open University, 2016). In the last 50 years, the world's need for water has grown four times bigger, reaching 4,000 cubic kilometers per year. This is about one-third of the water we

can use from rain. Numerous locations across the globe are depleting their water supplies, and many others are on track to face similar issues due to the rapid consumption of groundwater and surface water. There are various strategies to address this challenge. (Abdellatif, W. & Abdel Kader, S., 2023):

- Retain (collecting, preserving, and storing):
- Cut down on spills and demand.
- Reuse and recycle water.
- Reimagine technology to increase productivity.
- Low-cost brackish and seawater desalination.

Given the conditions, a vast number of plants are currently operating worldwide, turning 27.5 million m^3 of salty and seawater into fresh water daily. This represents just 3% of the drinking and sanitation water used worldwide.

Wastewater and seawater can be treated using a variety of technologies, including physical, membrane separation, chemical, and biological ones. The main disadvantages of chemical and biological treatments are their high treatment costs, the use of dangerous chemicals due to fossil fuels, and the setup space requirements. Membrane processing and thermal distillation are the two innovative desalination techniques that are now in use worldwide ((SIWI), 2020).

There are two categories of desalination technologies: membrane processes that utilize a membrane as a separating agent, and thermal methods, which eliminate water from the saline solution by means of evaporation of the remaining salt. Vapor compression (VC), multiple-effect distillation (MED), and multiple-stage flash evaporation (MSF) include thermal methodologies. Electrodialysis (ED) and reverse osmosis (RO) are techniques that utilize membranes. Membrane distillation (MD) is a pioneering method applicable for both desalination and recycling. (A. Marni Sandid et al., 2021).

Diverse strategies have been employed to generate vapor pressure over hydrophobic membranes. In every case, the heated side of the membrane directly contacts the unprocessed water necessitating desalination. In each membrane distillation process, A liquid input system interacts with a hydrophobic, microporous membrane. Membrane wetting transpires when a solution is unable to permeate the membrane's pores due to the membrane's hydrophobic characteristics. The membrane does not alter the vapor-liquid equilibrium; its role is to enhance the interaction between liquid and vapor. (Abu-Zeid et al., 2023).

The disparity in the partial vapor pressure of the species traversing a membrane is the primary catalyst for mass transfer across the membrane. This variation in partial vapor pressure can be generated by several methods, contingent upon the configuration of the MD system (Li, et al., 2019). During the process known as direct contact membrane distillation (MD), the feed solution and both surfaces of the membrane are brought into simultaneous contact with one another. The temperature of the feed solution must exceed that of the permeate solutions to create the necessary impetus for vapor migration across the membrane. If the aim of the technique is to retrieve salt from saline water, then freshwater acts as the permeating solvent, (Tijing et al., 2015). In air gap membrane distillation (MD), solely the feed water interacts directly with the membrane. The permeate accumulates on a chilled surface. A void is present between the membrane and the chilled surface to reduce energy dissipation caused by heat conduction through the membrane.

The air gap configuration poses a considerable constraint by hindering mass transfer efficacy. Air gap membrane distillation (AGMD) can be utilized in the same scenarios as direct contact membrane distillation (DCMD). AGMD surpasses DCMD in the elimination of volatile substances from liquid solutions. In DCMD, these components may increase moisture on the permeate-side membrane due to their lower surface tension and reduced contact with the membrane material. Conversely, AGMD circumvents this problem by ensuring that the permeate remains isolated from direct interaction with the membrane, hence inhibiting moisture buildup on the permeate side (Thakur, A. K. et al., 2020).

A method referred to as membrane air stripping is utilized in the sweep gas membrane distillation (SGMD) setup. A notable benefit of utilizing a sweep gas is its capacity to reduce resistance to mass transfer within the air gap. On the contrary, a fundamental problem is that the sweep gas diminishes the vapor phase, requiring additional energy for the condenser to efficiently retrieve the isolated components (Boukhriss, M. et al., 2020). Rather than employing sweep gas, vapor in Vacuum MD can be eliminated by evacuating it and allowing condensation from an external source (Viwanathan S. et al.).

This research is to investigate the (AGMD) method employed in desalination facilities for the generation of potable water. AGMD is distinguished by its distinctive design, which includes an air gap separating the condensation surface from a hydrophobic porous membrane (Fig. 1) (Shahroie et al., 2016). When the feed solution is heated, volatile substances like water vaporize at the liquid-vapor boundary of the membrane. The vapor released from the membrane permeates through the pores and into the air gap, where it cools and forms droplets on a surface incorporated into the membrane module (Tai Z. S. et al., 2023).

The disparity in vapor pressure differential across the membrane facilitates mass transfer.in (AGMD). The introduction of an air gap markedly diminishes thermal loss via the membrane substance, possibly improving permeate flow. Nonetheless, the existence of this air gap hinders vapor flow; bigger gaps lead to diminished flux owing to heightened mass transfer resistance. Modifying the breadth of the air gap could transition the predominant method of heat transmission from conduction and diffusion to natural convection. Establishing the correct dimensions for the air gap is essential for maximizing system performance, since narrower gaps diminish heat loss but could hinder vapor flow. In AGMD, vapor condenses on the cooling surface, so averting direct interaction between the liquid permeate and the membrane. This inhibits the membrane from becoming moist. This configuration offers a significant advantage in the

selective separation of target components from aqueous solutions, minimizing the risk of membrane contamination (Karanasiou, A. et al., 2018).

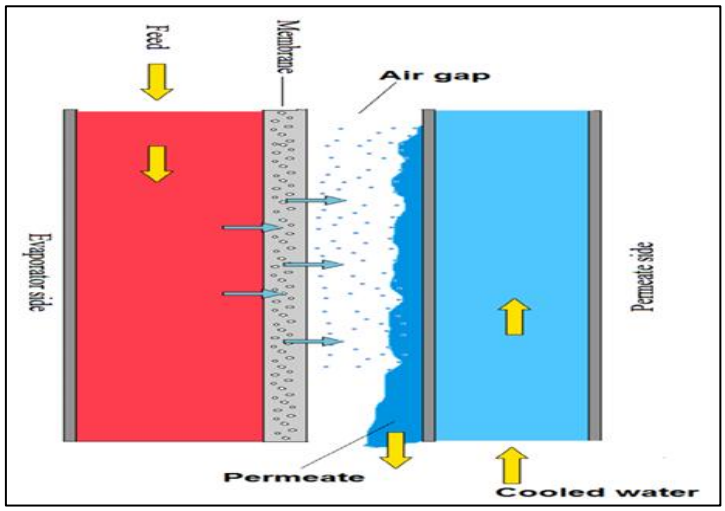


Figure 1: Air Gap Membrane Distillation (AGMD) Diagram . (Shahroie et al., 2016)

Membrane distillation process sophisticated thermal desalination technology that functions based on vapor pressure gradients instead of hydraulic pressure differentials. A heated saline solution traverses a hydrophobic membrane in this process. A thermal differential between the feed and permeate surfaces of the membrane induces the migration of water vapor through the membrane pores, where it condenses on the colder surface, resulting in a vapor pressure differential. The hydrophobic characteristics of the membrane inhibit the infiltration of liquid water while allowing vapor exchange, enabling almost total salt exclusion. An important benefit of MD is its effective operation at ambient pressure and moderate temperatures (40–90°C), which allows compatibility with sustainable energy sources like industrial waste heat or solar thermal systems. The primary energy requirement entails providing low-grade heat to facilitate water evaporation through the membrane, highlighting its potential for energy efficient desalination when combined with renewable or residual thermal resources (Qasim, M. et al., 2021).

The increasing demand for sustainable desalination technologies is underscored by the growing worldwide freshwater scarcity, global climate change, and population growth. The conventional methods, like reverse osmosis (RO) and thermal distillation (MSF/MED), require a significant amount of energy and rely on high-quality electricity or heat generated from fossil fuels, limiting their applicability in off-grid areas that face water shortages. For example, heating processes emit 15–25 kg CO_2 per m^3, combining environmental stresses, while RO requires 3–10 kWh/m^3 of desalinated water. By utilizing low-grade heat (less than 90°C) and integrating renewable energy, air gap membrane distillation (AGMD) becomes a viable option. However, its widespread adoption is hindered by insufficient energy recovery and a dearth of scalable hybrid designs (Bendevis et al., 2019).

By developing a solar-powered AGMD system with sensor-driven control in real-time and facultatively efficient use of intermittent solar energy, this work fills these gaps. Additionally, using off-grid heating sources fills a significant study gap by improving shortcomings in earlier AGMD studies that mostly focused on conventional heating sources and offering useful insights for energy-efficient implementation (Belessiotis, V. et al., 2016; Kabeel et al., 2019).

(Mohamed H Koura et al., 2025), examined the effects on system performance and production rate of replacing a conventional AGMD system with a flat coolant plate with a specially designed, portable channeled coolant plate. To maintain the system's portability, certain dimensions were chosen. The complete module is made up of five essential parts: The first five parts are a membrane ramp, a hot solution chamber, a fine coolant plate, an air gap frame, and a cold solution chamber. The hydrophobic membrane made of PTFE measured 150 μm in thickness, featured a pore dimension of 0.45 micrometers, and had a porosity of 85%. The feed and coolant temperatures of the system have been set at 40°C and 70°C and 10°C to 25°C, respectively. Because of its small size and efficiency, the module can provide more fresh water per unit of time, allowing the system to be utilized daily even in a home environment.

This research investigates the energy management of (AGMD) utilized in desalination systems via both theoretical and empirical approaches. Examining the operational variables including flow rate, temperature, and pressure, along with the hybrid system using PV solar cells, affect water productivity from the setup, a test rig has been designed and constructed for experimental analysis, (Mohamed H Koura et al., 2025). Temperature (40–70°C), pressure (0.5–1.0 bar), and flow rate (1–2 L/min) are the operating parameters under study. In the theoretical study, MATLAB is used to model the AGMD system to examine how various operating factors affect the system's energy management. comparing the current model's results with existing prior research.

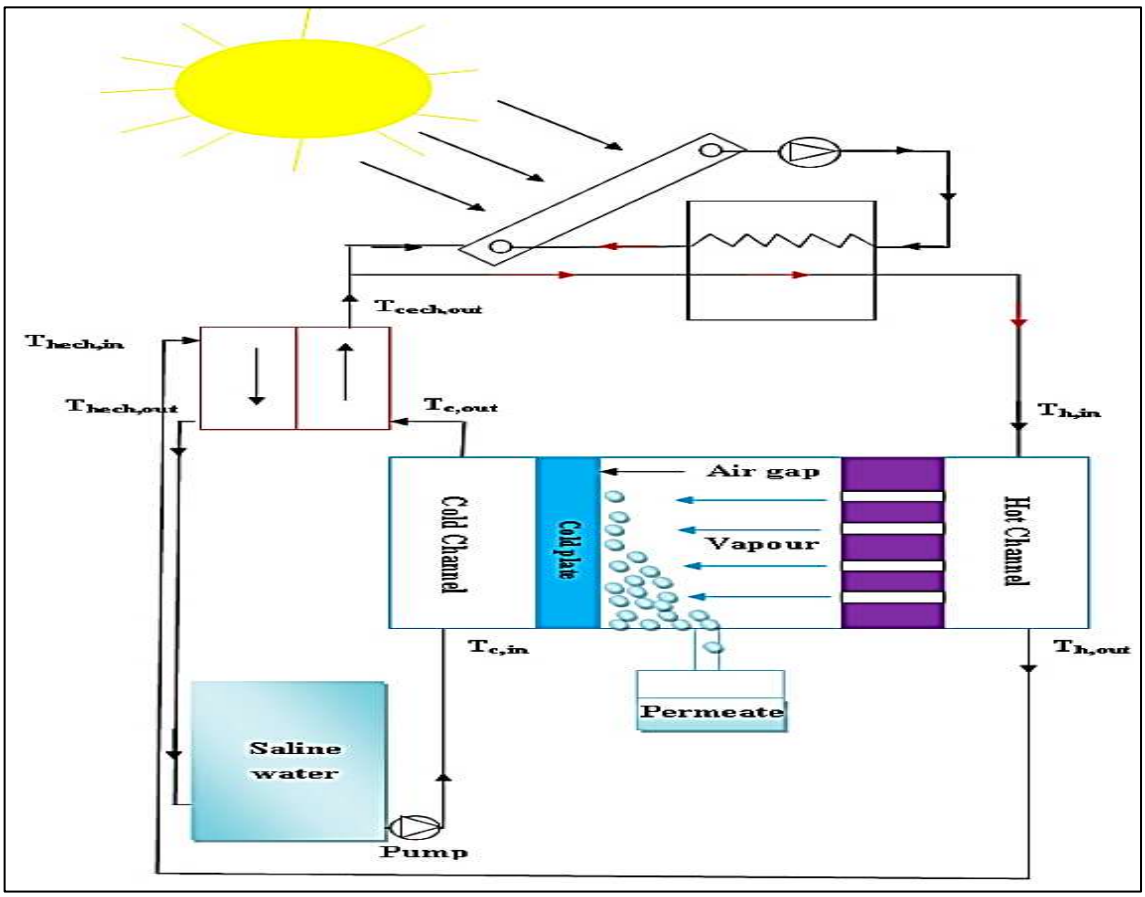


Figure 2: Schematic diagram and components of a small solar AGMD system. (Mouche, M. et al., 2023)

By combining a flat-plate solar collector for heating sources with real-time flow/temperature control via Arduino sensors, this study offers a solar-driven AGMD system with enhanced energy management, Fig. 2 (Mouche, M. et al., 2023). This work incorporates energy and economic assessments to evaluate performance holistically, in contrast to previous AGMD studies that focused only on thermal efficiency. Additionally, at a temperature of feed of 70°C, a 44.49% thermal efficiency is attained, which is 23.89% more efficient than standard on-grid AGMD installations that rely on conventional nonrenewable heating sources.

While (AGMD) shows promise for sustainable desalination, current research faces several critical challenges:

- Limited Renewable Energy Integration: Most AGMD studies focus on conventional energy sources, with minimal investigation into solar-powered, off-grid setups.
- Absence of Dynamic Control Systems: Few AGMD systems employ intelligent, sensor-driven controls to adapt to fluctuating solar energy or feedwater conditions, limiting efficiency and responsiveness.
- Incomplete Performance Assessments: Existing research often prioritizes thermal efficiency or permeate flux in isolation, lacking holistic techno-economic analyses that account for (STEC), (GOR), and (CPL).
- Inadequate Model Validation: While some AGMD models exist, rigorous experimental validation across diverse operating conditions remains scarce, hindering their reliability for scaling.

To address these constraints, this research presents the subsequent innovations:

- A validated MATLAB-based AGMD model, calibrated with experimental data to enhance accuracy and scalability.
- A solar-powered AGMD prototype with a flat-plate solar collector and Arduino-controlled adaptive operation, optimizing energy use under real-world solar variability.
- A detailed energy and economic evaluation, achieving a competitive CPL of \$2.52/m³ and STEC as low as 29.04 kWh/m³.
- Improved thermal efficiency (44.49%), surpassing conventional AGMD systems dependent on fossil fuels.

These innovations support the development of decentralized, cost-effective desalination design for remote and scarce water areas, making a meaningful step toward sustainable water solutions.

2. Modeling and Simulation

Water vapor infiltrates a hydrophobic microporous membrane and condenses on a cooled surface, separated by an air gap in the (AGMD) process, acknowledged as a thermally induced separation method, as illustrated in the fundamental framework of the AGMD system seen in Figure 6. The model incorporates mass and heat transport mechanisms, utilizing the Knudsen–molecular diffusion approach (Perves Bappy, M. J. & Bahar, R., 2022), applicable when the Knudsen number lies between 0.01 and 1, to determine the vapor flux. The movement of water vapor (***J***) is propelled by the disparity in vapor pressure between the cooling side and the feed side, calculated by a composite resistance model that include both air gap resistance (R_a) and membrane resistance (R_m).

R_m considers the membrane's thickness, porosity, tortuosity, and pore dimensions. The efficient thermal conductivity (k_m), influenced by the membrane's porosity and material characteristics, is used to model heat transfer across the membrane, incorporating both the latent heat of vaporization and conductive heat dissipation through the membrane framework.

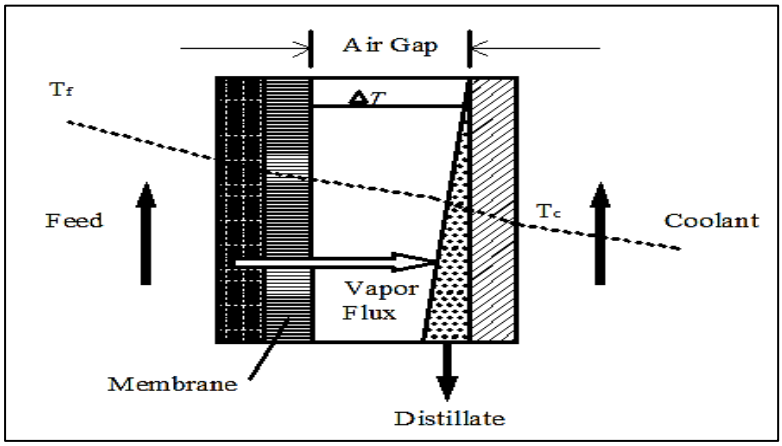


Figure 3; AGMD system basic model.

To assess the effectiveness of the system, performance metrics such as (STEC), (GOR), thermal efficiency (TE), and permeate flux (Jp) are determined. The equations for these parameters are presented below (Perves Bappy, M. J. & Bahar, R., 2022), and used to build a MATLAB simulation code.

2.1 Transportation of Vapor in AGMD

Antoine's correlation for pure water may be utilized to articulate the AGMD procedure's vapor movement in terms of temperature, where:

$$\log P_w = A - [(B/(C + T_w)] \quad (1)$$

where P_w is pressure of vapor and T_w is temperature for distilled water, in which the motivating potential:

$$\Delta P = P_{w1} \sim P_{w2} \quad (2)$$

where the components ***A***, ***B***, and ***C*** are particularly constant for distilled water. Using Raoult's law, the value of P_w for saline water is adjusted as follows:

$$P_w = (1 - CM_{NaCl}) P_{\text{pure water}} \quad (3)$$

where the mole solute concentration is represented by CM_{NaCl}.

The component's concentration now determines the diffusion rate across the membrane. The mass flow of a substance per unit area is intricately linked to the fluctuations in concentration., which is indicated by Fick's Law.

$$\dot{m}_A/A = -D \times \left(\partial C_A/\partial x\right) \quad (4)$$

where C_A denotes the mass concentration of component ***A*** per unit volume, $\dot{m}_A$ denotes the mass flow rate per unit of time, while ***D*** represents the diffusion constant. Once more, the total mass transfer of water vapor is dictated by Stefan's diffusion equation:

$$\dot{m}_{W,total} = \frac{D_P M_w A}{R_o T(X_2 - X_1)} \quad (5)$$

where A signifies the total surface area, D_P represents the diffusion coefficient, M_w indicates the molecular weight of water, R_o stands for the universal gas constant, T pertains to the temperature, and $X_2 - X_1$ defines the air thickness. (distance to be traveled).

2.2 *Transfer of Mass and Heat Across an Air gap*

The theory of molecular diffusion explains the transfer of vapor across the air gap and through the pores of membranes. In the AGMD system, it is presumed that a stagnant air film exists within the air gap. Vapor molecules are transported through this still air region by means of laminar flow, which takes place during molecular diffusion. The diffusion rate can be ascertained by Fick's law of diffusion:

$$N_v = -D\frac{dC_v}{X} \quad (6)$$

where D represents the diffusivity, C_v indicates the concentration of vapor, X denotes the distance of the air gap, and N_v refers to the rate at which the vapor molecules move through the air gap. A negative correlation appears when the air gap widens, while the vapor concentration diminishes.. Equ. (7) (Perves Bappy, M. J. & Bahar, R., 2022) This can be utilized to characterize the flux through the membrane and across the air gap for unidirectional flow if the air gap does not exceed 5 mm in length.

$$J = \frac{\mathrm{PM}}{\mathrm{RTP_w}}\left(\frac{D}{\frac{\delta}{\varepsilon^{3.6}}+1}\right)\Delta p \quad (7)$$

In this context, Δp represents the variance in vapor pressure between the surface of condensation and the feed of the membrane. The water's partial pressure is indicated by $\mathrm{P_w}$. To calculate the overall mass transfer of water vapor through an air gap, Stefan's law of molecular diffusion can be applied. (Perves Bappy, M. J. & Bahar, R., 2022):

$$\dot{M}_{w,total} = \frac{\mathrm{DPM_w}A}{RTX}\frac{dP_w}{dy} \quad (8)$$

where D represents the diffusion coefficient, X denotes the air gap, and A refers to the area. The influence of natural convection in the air gap on the vapor movement throughout it is minimal as well. Natural convection occurs because of the thermal gradient across the gap. Rayleigh number R_a assesses the importance of natural convection. (Perves Bappy, M. J. & Bahar, R., 2022):

$$R_a = \frac{\mathrm{g\beta\Delta T_x \delta_x^3}}{\nu_\mathrm{a}\alpha_\mathrm{a}} \quad (9)$$

According to Equation (9), ν_a and α_a denote the kinematic viscosity and thermal diffusivity of air, respectively. ΔT_x represents the temperature differential across the air gap, whereas δ_x indicates the thickness of the air gap. The coefficient of thermal expansion is denoted by β, while g signifies gravitational acceleration. The analysis indicates that natural convection can be overlooked in favor of conductive heat transfer via the air gap when the Rayleigh number (R_a) is under 1,000. (Perves Bappy, M. J. & Bahar, R., 2022).
The subsequent equation represents the conductive heat transport within the interstice:

$$Q = \left(\frac{K_a A}{t} + \dot{m}c\right)\Delta T \quad (10)$$

Here, A signifies the effective area for thermal exchange, $\dot{m}$ represents the mass flow rate, ΔT depicts the temperature differential across the air gap, and K_a refers to the thermal conductivity of atmospheric air.

The outcomes of the simulation show that while increased porosity and reduced tortuosity improve both flux and thermal performance, higher feed temperatures and thinner membranes improve vapor flux. This model offers a solid foundation for examining the impacts of design and operating factors in AGMD systems, and it was validated using parameters that align with experimental investigations employing PTFE membranes (Mohamed H Koura et al., 2025).

3. Parameters of AGMD Thermal Performance

A range of performance indicators is utilized to evaluate the efficacy of the MD process. The main performance metrics evaluated in this research are (STEC), (GOR), (Jp), and (TE). Permeate flux functions as a benchmark for

evaluating efficiency in membrane distillation (MD) systems. This denotes the quantity of water that passes via a unit area of the membrane over a specified time. The equation provided determines permeate flow by dividing the cumulative volume of water vapor gathered throughout the procedure by the functional surface area of the membrane. (Zhou, Y. et al., 2023; Boubakri et al., 2020):

$$Jp = \frac{m_p}{S\Delta t} \tag{11}$$

Thermal efficiency (TE) refers to the proportion of heat transferred by the vapors compared to the total heat that is carried over by the microporous membrane (Zhou, Y. et al., 2023; Boubakri et al., 2020):

$$TE = \left[{J_p \Delta H_V} \Big/ {J_p \Delta H_V + \left(\frac{k_m}{\delta}\right)(T_{fm} - T_{pm})} \right] \times 100 \tag{12}$$

The equation provided calculates the GOR to evaluate the thermal efficacy of the AGMD procedure (Boukhriss, M. et al., 2018; Duong, et al., 2016):

$$GOR = {F_d S \rho_d \Delta H_V} \Big/ {F_f \rho_f C_{p,f} (T_{f,in} - T_{p,out})} \tag{13}$$

It is possible to compute the STEC of the AGMD process by using the formula that is presented below. This formula represents the amount of heat energy that is necessary to generate one milliliter of distillate (Zhou, Y. et al., 2023; Boubakri et al., 2020):

$$STEC = {F_f \rho_f C_{p,f} (T_{f,in} - T_{p,out})} \Big/ {3.6 \times 10^6 F_d} \tag{14}$$

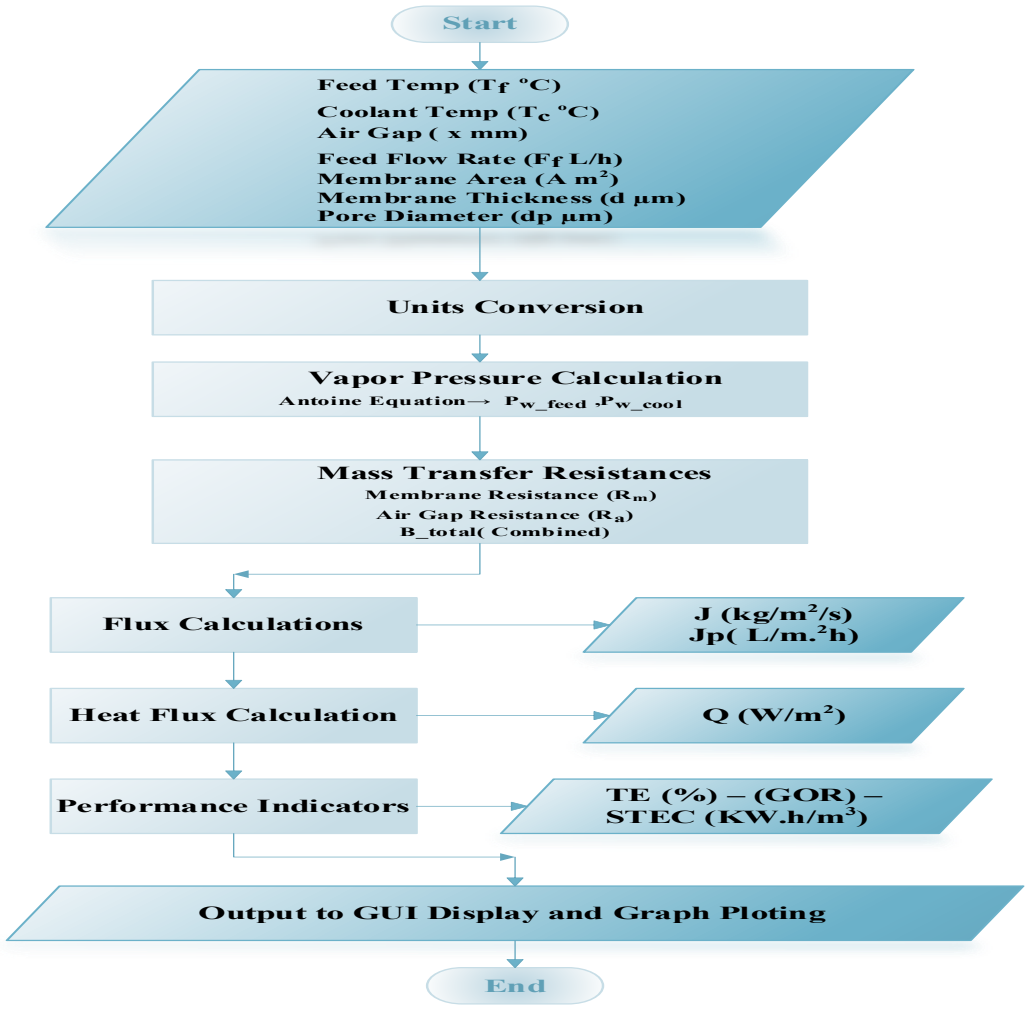


Figure 4; Flow Chart of AGMD MATLAB Code.

4. Cost Analysis

Increasing freshwater output while lowering the cost per liter of freshwater generation is the primary goal of solar-powered distillation systems. Therefore, the following methods are used to evaluate distillation systems that have been subjected to economic analysis:

The following equation computes Capital Recovery Factor (CRF), (Z. Zhang et al., 2022; Bartholomew et al., 2020).

$$\mathbf{CRF} = \frac{\boldsymbol{i}(\mathbf{1}+\boldsymbol{i})^{\boldsymbol{n}}}{(\mathbf{1}+\boldsymbol{i})^{\boldsymbol{n}}-\mathbf{1}} \tag{15}$$

where n is the AGMD's lifetime years, or five years, and i is the yearly rate of interest, which is around 12%.

The system's primary expense is the solar distillation unit is first annual cost (FAC), which may be found using the following formula, (Z. Zhang et al., 2022; Bartholomew et al., 2020):

$$\mathbf{FAC} = \mathbf{CRF} \times \mathbf{P} \tag{16}$$

where the capital cost is denoted by P. The following formula provides the AGMD one unit is annual cost of salvage value (ASV), (Z. Zhang et al., 2022; Bartholomew et al., 2020):

$$\mathbf{ASV} = \mathbf{SSF} \times \mathbf{S} \tag{17}$$

In this context, SSF refers to a system's sinking fund factor (SFF), while S denotes the salvage value of the AGMD. The subsequent equation describes S, (Z. Zhang et al., 2022; Bartholomew et al., 2020):

$$\mathbf{S} = \mathbf{0.2} \times \mathbf{P} \tag{18}$$

The following equation provides SSF, (Z. Zhang et al., 2022; Bartholomew et al., 2020):

$$\mathbf{SSF} = \frac{\boldsymbol{i}}{(\mathbf{1}+\boldsymbol{i})^{\boldsymbol{n}}-\mathbf{1}} \tag{19}$$

The anticipated annual maintenance expense (AME) is projected to be 15% of the initial yearly cost. (Z. Zhang et al., 2022; Bartholomew et al., 2020):

$$\mathbf{AMC} = \mathbf{0.15} \times \mathbf{FAC} \tag{20}$$

This following formula provides the AGMD unit is total yearly cost, (Z. Zhang et al., 2022; Bartholomew et al., 2020):

$$\mathbf{AC} = \mathbf{FAC} + \mathbf{AMC} - \mathbf{ASV} \tag{21}$$

Finaly, the cost per liter (CPL) of the freshwater yield is determined by, (Z. Zhang et al., 2022; Bartholomew et al., 2020):

$$\mathbf{CPL} = \frac{\mathbf{AC}}{\mathbf{P_n}} \tag{22}$$

where Pn is the water production per year. A comparison was made between the product's cost in this study and the cost determined in Table (1) by Zhang et. al. (Z. Zhang et al., 2022) & Bartholomew et al. (Bartholomew et al., 2020). The product's current cost in the system is more cost-effective.

Table 1: Expense of the Product for Current and Prior Researches

Research	Current work	Literature Zhang et.al. (Z. Zhang et al., 2022) & Bartholomew et al. (Bartholomew et al., 2020)
	5 mm Gap	
Cost per Liter CPL($)	0.00248 $/l	0.00277 $/l
Cost per m^3 ($)	2.52 $/$m^3$	2.77 $/$m^3$

This cost is competitive when compared to conventional desalination in remote or off-grid areas (typically between 1.5–3.0 USD/m³ depending on energy source and scale) (Z. Zhang et al., 2022; Bartholomew et al., 2020).

5. Model Results

A variety of model trajectories are analyzed for both feed and coolant fluids at different feed and coolant temperatures, while keeping a steady flow rate of 2 L/min. The coolant temperature must be between 10 and 25 °C, allowing for a 5-degree variance, while the feed temperature should be maintained between 40 and 70 °C, also with a 5-degree tolerance. Nevertheless, the air gap possesses a mere thickness of 5 mm.

Table 2 presents a sample of data collected through modeling. Figure 5 demonstrates the variation in permeate flux (Jp) at various feed temperatures with a flow rate of 2 L/min. In alignment with results from prior AGMD research. (Mohamed H Koura et al., 2025). The Antoine equation clarifies the observed nonlinear increase in permeate flow corresponding to rising feed temperatures. This relationship indicates that vapor pressure increases nonlinearly with rising temperature, thereby enhancing the force that drives mass movement. This augmentation intensifies the temperature differential across the membrane and elevates the diffusion coefficient. Elevated temperatures diminish the viscosity of the feed solution, thereby improving mass transfer efficiency. The findings indicate that increased feed temperatures result in greater distillate production. The highest distillate flow rate observed was 12.77 kg/m²·h, attained at a feed temperature of 70°C and a coolant temperature of 10°C. The lowest flow recorded is 1.75 kg/m²·h, which takes place at a feed temperature of 40°C and a coolant temperature of 25°C. The findings illustrate the importance of thermal gradients in improving the efficacy of membrane distillation.

Table 2: Summary of Model Results

	Distillated Flux Kg/m².h			
Temp. °C	10	15	20	25
70	12.77	12.67	12.51	12.25
65	10.06	9.94	9.76	9.48
60	7.84	7.71	7.51	7.21
55	6.04	5.89	5.67	5.37
50	4.58	4.42	4.20	3.88
45	3.42	3.25	3.02	2.69
40	2.49	2.32	2.08	1.75

The distillated flux tends to diminish when the temperature of feed is reduced to 40°C also, when the coolant temperature is increased to 25°C. These findings suggest that optimal distilled flow can be obtained by setting the operating parameters to a maximum temperature of feed of 70°C and a minimum temperature of coolant of 10°C.

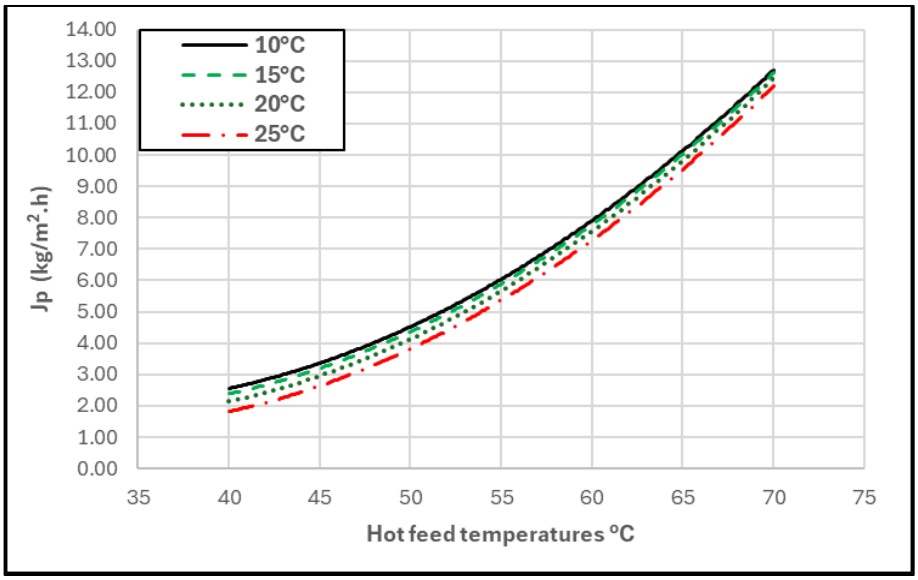


Figure 5: Model Distillated Flux vs Feed Temperature for Different Coolant Temperatures.

6. Efficiency of the AGMD Model in Terms of Thermal Energy

Significant metrics like (STEC) are employed to assess the efficacy of (AGMD) systems. (TE) denotes the proportion of thermal energy employed for the vaporization of water through the membrane relative to the overall heat input. Enhancing the efficacy of AGMD necessitates an emphasis on minimizing conductive heat dissipation via the polymer membrane, as this significantly influences thermal efficiency. Enhancing thermal efficiency ensures that a greater proportion of the heat generated is utilized for vapor production, thereby improving the overall energy utilization of the system (Boukhriss, M. et al., 2021).In membrane distillation (MD) desalination, thermal energy consumption (TE) denotes the amount of heat necessary to raise saltwater to the suitable operational temperature. Figure 6 depicts the fluctuation of TE as a function of alterations in feed input temperature. Increasing the feed temperature from 40°C to 70°C enhances the thermal efficiency from 30.55% to 50.62%, corroborating results from additional research. (Nakoa et al., 2015). This aligns with previous observations: elevated feed temperatures enhance the energy efficiency of thermal-driven desalination systems by increasing vapor pressure gradients, thereby optimizing heat utilization for water evaporation (Zhou, Y. et al., 2023; Boubakri et al., 2020). Fig. 6 highlights that at higher feed temperatures, latent heat loss constitutes over 40% of the total thermal energy input required for vaporization. Higher feed temperatures lead to an increase in permeate flow, subsequently raising the latent heat required for water evaporation. The energy necessary for vaporization surpasses the conductive heat losses via the membrane, leading to considerable latent heat inefficiencies at higher operational temperatures.

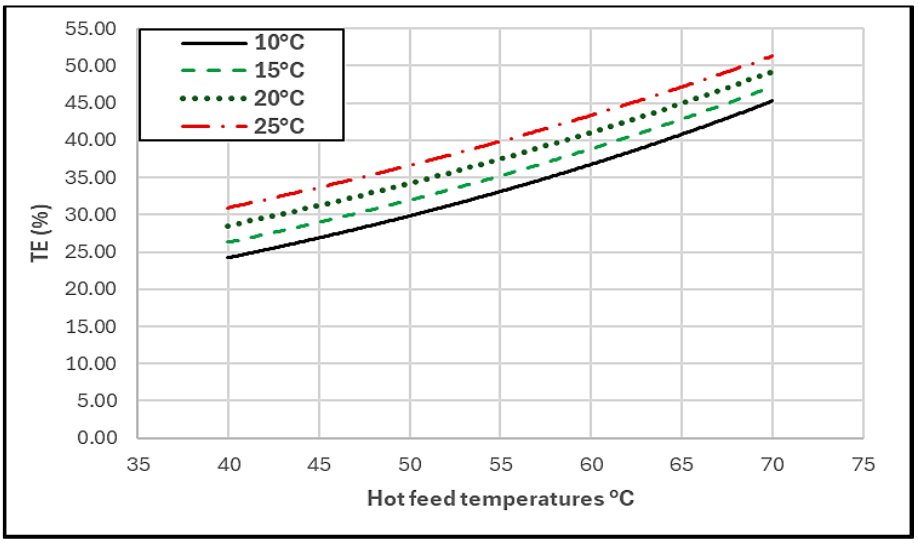


Figure 6:Influence of the feed inlet temperature and coolant feed temperature on the model's thermal performance efficiency.

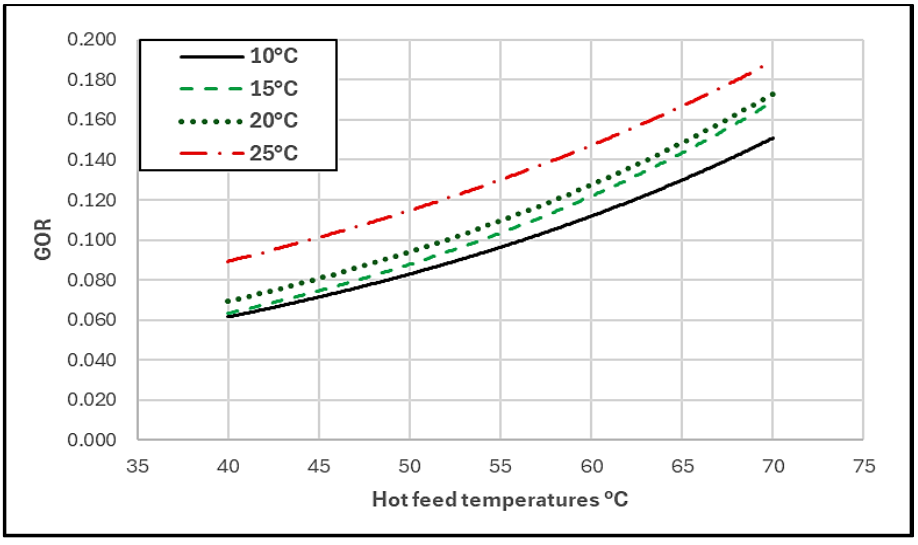


Figure 7:Influence of the feed inlet temperature and coolant feed temperature on Model GOR.

Fig. 7 illustrates the alteration of GOR with differing feed inlet temperatures. It has been shown that while the input temperature oscillates between 40 and 70°C, the GOR increases by 60%; still, the maximum GOR of 0.191 is much inferior to that of alternative desalination techniques.

The alteration in STEC relative to the feed intake temperature, as illustrated in Fig. 8, indicates a reduction in STEC from 90.31 to 29.04 kW.h/m^3 when the temperature escalated from 40 to 70°C. A multitude of research efforts have demonstrated a comparable decline in STEC (Zhou, Y. et al., 2023; Boubakri et al., 2020) & (Boukhriss, M. et al., 2021). The reduction in STEC at higher temperatures can be explained using the Antoine equation, which elucidates the relationship between temperature and vapor pressure. As a result, elevated temperatures result in a rise in vapor pressure, hence diminishing the energy needed.

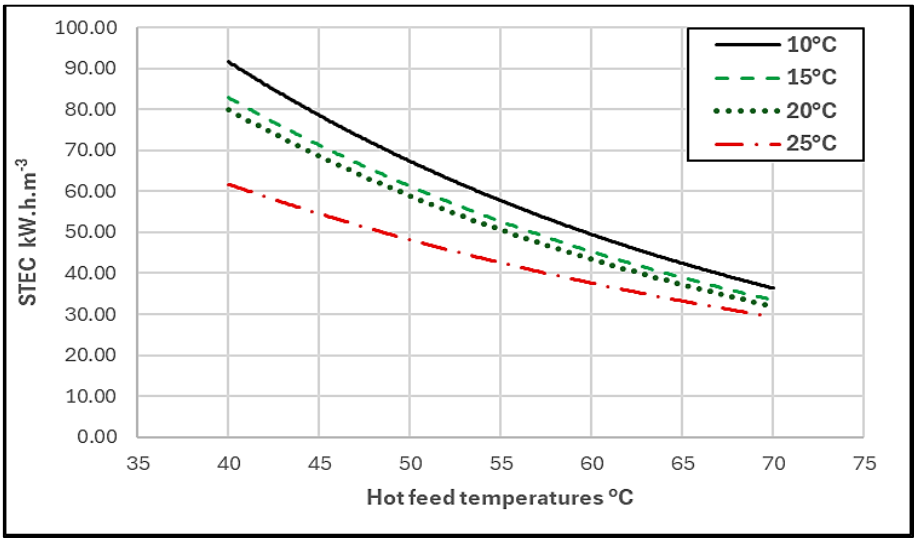


Figure 8: Influence of the feed inlet temperature and coolant feed temperature on Model STEC.

7. Comparison Between Previous Experimental Results and Modeling Data with Earlier Research

Model outcomes are obtained via experiments and analyzed alongside Koura et. al. (Mohamed H Koura et al., 2025), to validate the accuracy of the data collected under identical operating conditions. The data from the model are juxtaposed with the findings of (Mohamed H Koura et al., 2025) thru initial investigation, followed by validation against previous research (El Mokhtar, I. et al., 2019). Both researches and model data exhibit congruent trends and behaviors, as illustrated in Figures 9, 10, 11, and 12, which represent the (Jp), (TE), (GOR), and (STEC) concerning varying feed temperatures.

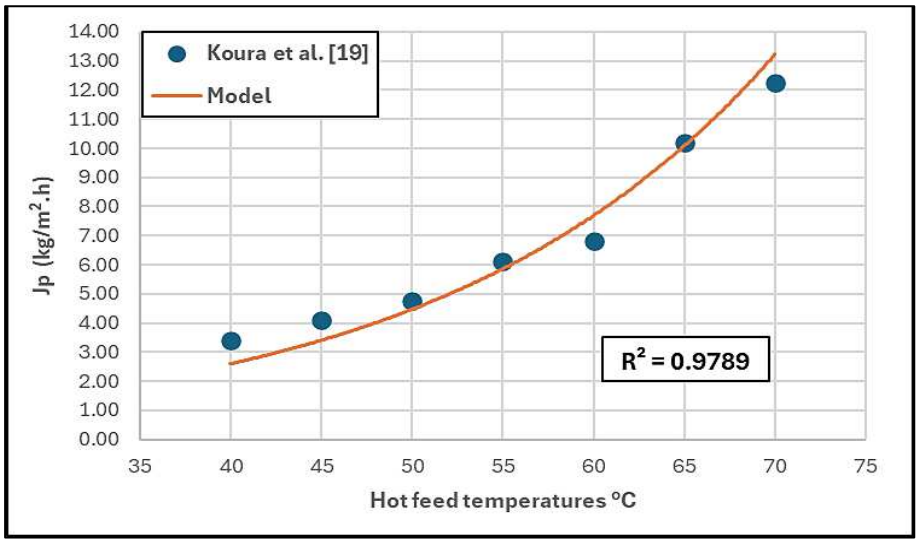


Figure 9: Validated Distillated Flux vs Feed Temperature for 10°C Coolant Temperature

Figure 9 illustrates a comparison between simulated data and empirical findings regarding permeate flux (Jp) at a fixed coolant temperature of 10°C in relation to feed temperature. The model precisely reflects the exponential rise in flux as feed temperatures increase, due to augmented vapor pressure differentials across the membrane. These findings corroborate the dependability of the Knudsen–molecular diffusion model and align well with the experimental data presented by (Mohamed H Koura et al., 2025).

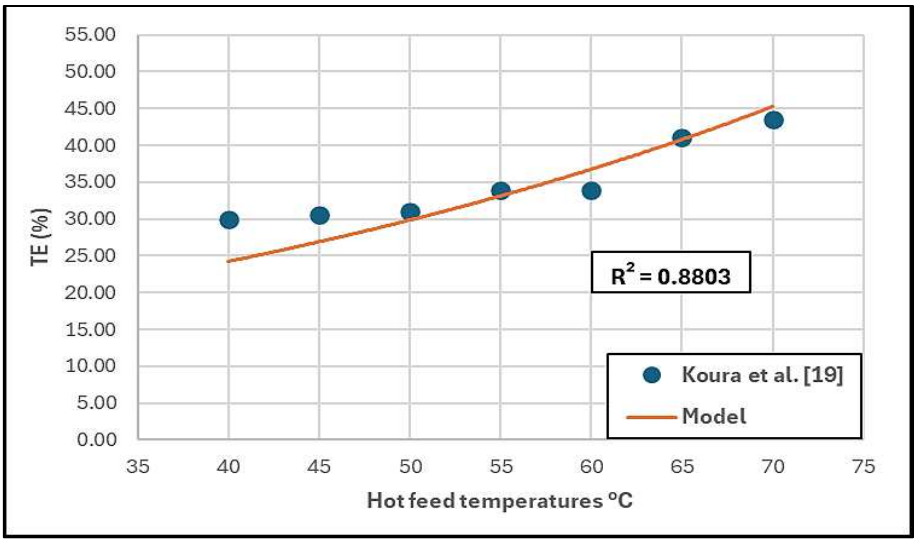


Figure 10; Validated TE vs Feed Temperature for 10°C Coolant Temperature.

Figure 10 shows that Thermal efficiency (TE) trends predicted by the model compared to experimental results at 10°C coolant temperature. The increasing TE with higher feed temperatures reflects more effective utilization of input heat for vapor generation, due to higher latent heat transfer and reduced relative conductive losses. The model shows a high degree of alignment with the measured data from (Mohamed H Koura et al., 2025), supporting its accuracy in simulating heat transfer dynamics in AGMD systems.

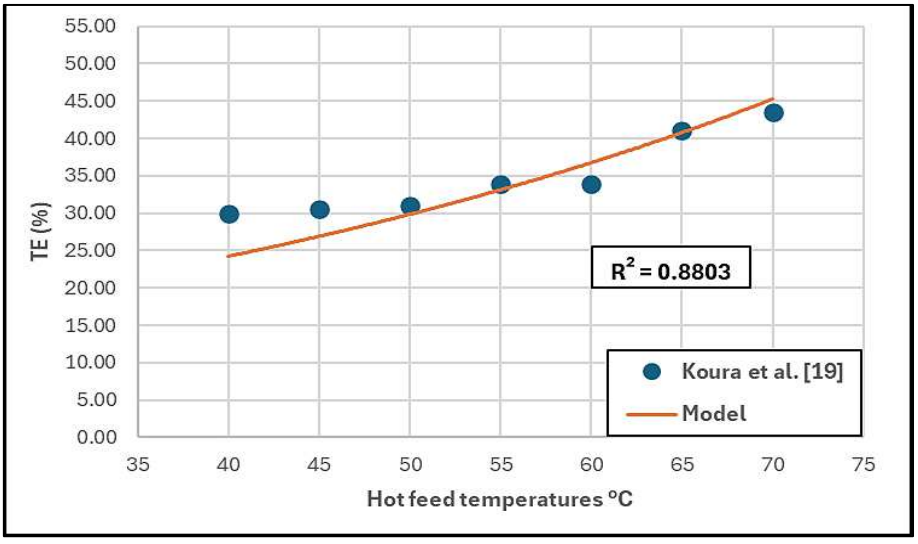


Figure 11; Validated GOR vs Feed Temperature for 10°C Coolant Temperature.

Figure 11 illustrates the (GOR) as a function of feed temperature at a coolant temperature of 10°C, comparing numerical calculations with empirical data. The model demonstrates a consistent rise in GOR with increasing feed temperature, attributed to improved thermal recovery and vapor production efficiency. The close match with (Mohamed H Koura et al., 2025) results indicates robust modeling of energy recycling performance within the AGMD configuration.

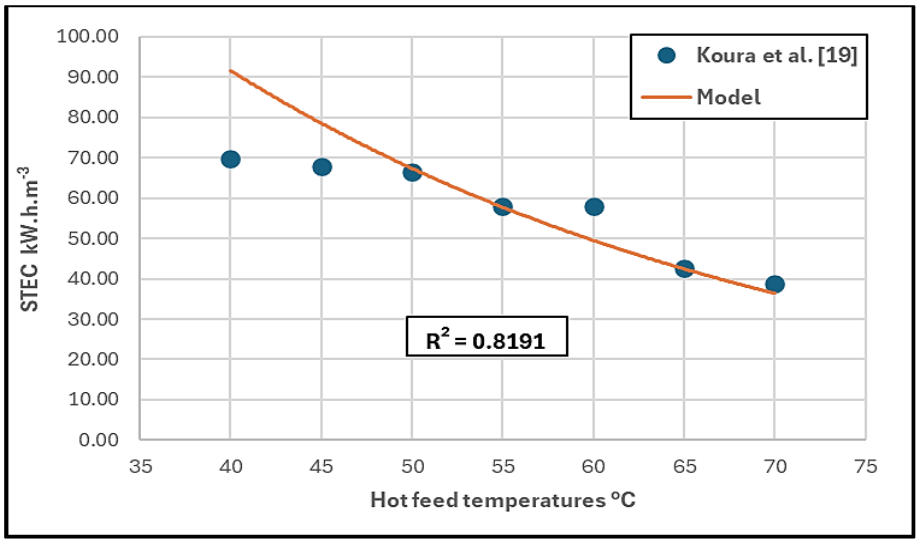


Figure 12; Validated STEC vs Feed Temperature for 10°C Coolant Temperature.

Figure 12: Validation of (STEC) trends versus feed temperature at 10°C coolant condition. The model effectively predicts the observed decrease in STEC with higher feed temperatures, a result of increased vapor pressure and improved energy utilization. These results confirm the model's suitability for evaluating energy efficiency in AGMD systems and correlate well with the experimental data of (Mohamed H Koura et al., 2025). Figures 9, 10, 11 and 12 showed that for different feed temperature changes the same behavior is obvious to take the same trend for Jp, TE, GOR and STEC curves with (Mohamed H Koura et al., 2025), experimental work. Figures 13, 14, 15, and 16 illustrate validation between model data and (El Mokhtar, I. et al., 2019) research verses different feed temperatures, showing Jp, TE, GOR and STEC behavior for them.

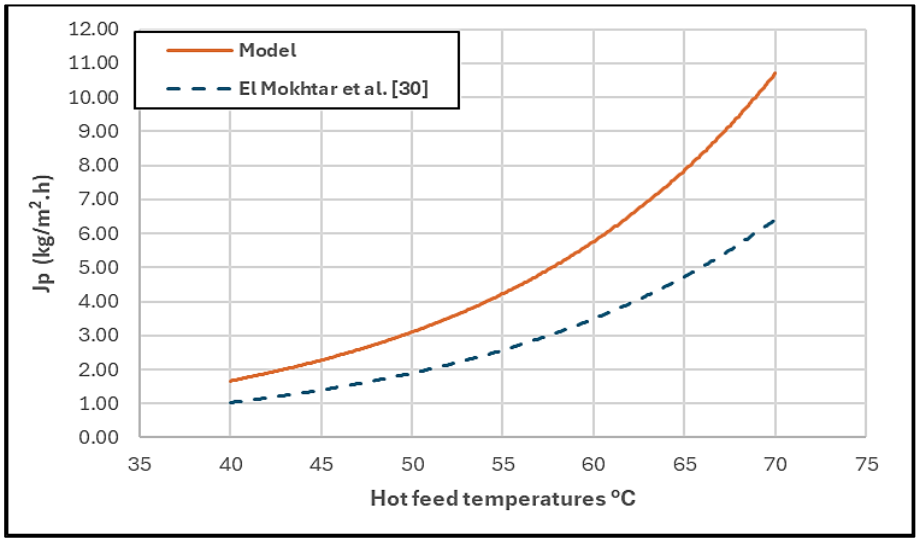


Figure 13; Validated Distillated Flux vs Feed Temperature for 23 °C Coolant Temperature.

Figure 13 depicts a comparison between modeled and experimental (Jp) data at a coolant temperature of 23°C relative to feed temperature. The model replicates the increasing flux trend with rising feed temperature, driven by elevated vapor pressure differentials and reduced feed viscosity. The strong agreement with (El Mokhtar, I. et al., 2019) confirms the model's robustness under higher coolant temperature conditions, where reduced thermal gradients slightly limit Jp.

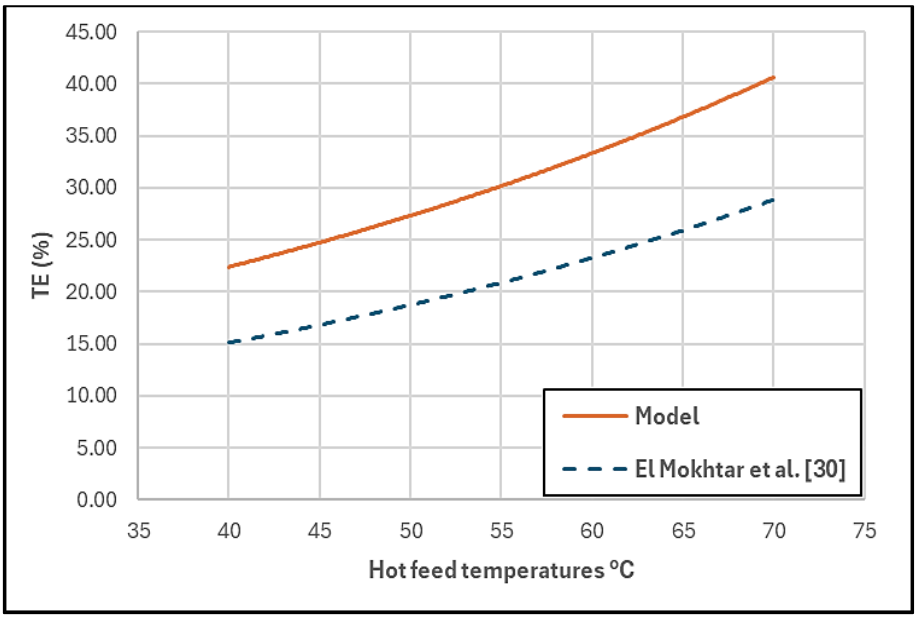


Figure 14; Validated TE vs Feed Temperature for 23 °C Coolant Temperature.

Figure 14 demonstrates Thermal efficiency (TE) variation with feed temperature at 23°C coolant temperature, showing strong alignment between modeled and experimental results. The gradual rise in TE reflects improved heat utilization as the feed temperature increases, albeit with a reduced slope compared to lower coolant conditions. Agreement with (El Mokhtar, I. et al., 2019) demonstrates the model's reliability in representing thermodynamic behavior under moderate thermal gradients.

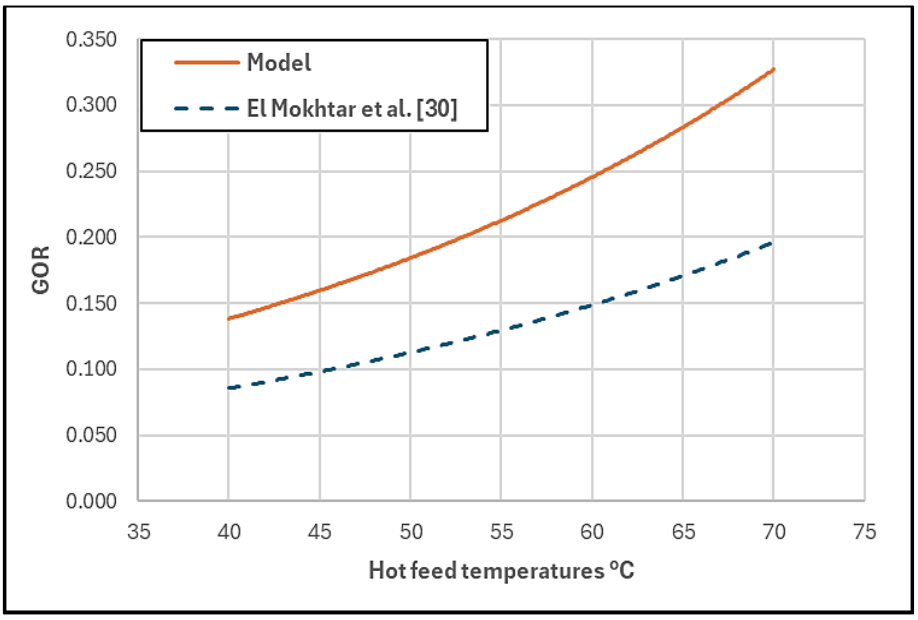


Figure 15; Validated GOR vs Feed Temperature for 23 °C Coolant Temperature.

Figure 15 displays Gained Output Ratio (GOR) plotted against feed temperature for a coolant temperature of 23°C. The model shows a consistent upward trend in GOR, consistent with experimental data from (El Mokhtar, I. et al., 2019), indicating increased thermal recovery with higher feed energy input. This supports the model's validity in predicting performance under reduced energy recovery scenarios at higher coolant baselines.

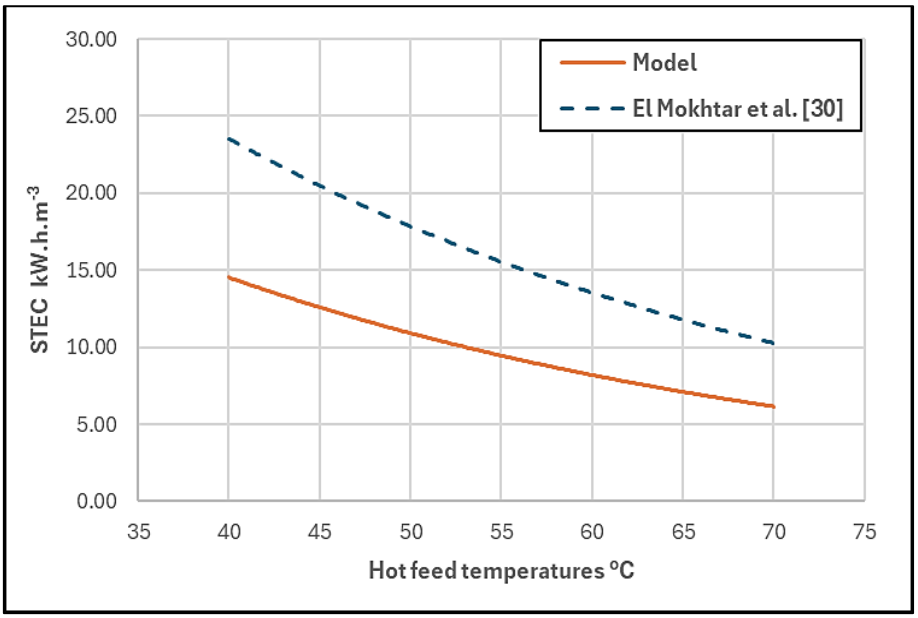


Figure 16; Validated GOR vs Feed Temperature for 23 °C Coolant Temperature.

Figure 16 expresses (STEC) versus feed temperature at a coolant condition of 23°C. The model precisely predicts the negative correlation between STEC and feed temperature, where decreasing values signify improved energy efficiency. These results closely mirror those of (El Mokhtar, I. et al., 2019), validating the model's effectiveness for energy analysis across varied operating conditions. From validated figures 13, 14, 15 and 16 showed the same behavior and trend between the model data and literature (El Mokhtar, I. et al., 2019), for each of Jp, TE, GOR and STEC curves. The validation results presented in Figs. 9 –16 indicate a strong correspondence between the experimental data reported by (Mohamed H Koura et al., 2025) and (El Mokhtar, I. et al., 2019) and the current outputs from the MATLAB simulation. For instance, the model successfully predicts the reduction in (STEC) and the rising trends in (Jp), (TE), and (GOR) as the feed temperature increases from 40°C to 70°C. The Antoine equation, demonstrating the exponential rise of vapor pressure with temperature and directly affecting the impetus for mass transfer, is a fundamental thermodynamic principle that regulates membrane distillation and corresponds with these observed patterns. Correctness of the transport models are validated by Figs. 9 and 13, which show that Jp increases exponentially with feed temperature in both the current model and previous research. Similarly, comparable improvements in TE and GOR (Figs. 10, 11, 14 and 15) indicate better thermal energy conversion and latent heat usage. The model's reliability in assessing thermal demand under varied circumstances is further supported by the STEC trends in Figs. 12 and 16, which show a noteworthy degree of consistency. These findings highlight the model's overall dependability and robustness. As a predictive and useful tool for system improvement, the AGMD simulation is validated by the close alignment across all four performance indicators (Jp, TE, GOR, and STEC) and different operating situations. This high degree of consistency not only validates the theoretical formulations used (such as Raoult's law and Knudsen-molecular diffusion), but it also shows how reproducible and scalable the suggested AGMD design is.

Conclusion

This study combined theoretical modeling with empirical experiments to create and verify a solar powered (AGMD) system. The results demonstrate that refining operational parameters, particularly elevating the feed temperature and lowering the coolant temperature, markedly improves system efficacy, detailed as follows:

- The AGMD system outperformed various thermal desalination techniques, with a peak permeate flux of 12.77 kg/m²·h and a thermal efficiency of 44.49% at a feed temperature of 70°C and a coolant temperature of 10°C.
- The (STEC) was minimized to 29.04 kWh/m³, confirming efficient energy utilization.
- The model's accuracy and prediction power are confirmed by its strong association with experimental findings and earlier studies (Mohamed H Koura et al., 2025) & (El Mokhtar, I. et al., 2019).
- These validations show that the system can be successfully scaled for real-world applications, which in turn boosts confidence in the underlying thermodynamic and transport principles. Additionally,
- This AGMD arrangement is competitive when compared to small-scale reverse osmosis systems, especially in off-grid or water-scarce areas, given its estimated water production cost of $2.52/m³.
- This AGMD framework offers a sustainable, economical, and ecologically friendly approach to freshwater production by utilizing solar energy and real-time sensor-driven control.

- Its proven dependability and effectiveness, it is a desirable choice for use in remote or decentralized desalination applications where traditional systems might not be feasible or cost-effective.
- The study advances the AGMD field by addressing three major research gaps:
    - Integration with renewable energy through solar collectors,
    - Implementation of adaptive, sensor-driven control systems,
    - A techno-economic evaluation including CPL and STEC metrics.
- These contributions position the proposed AGMD system as a viable, eco-friendly, and cost-effective alternative for freshwater production in water-scarce and remote regions.
- Future research should explore hybrid configurations, further reductions in thermal losses, and integration with energy storage systems to enhance round-the-clock performance.

References

(SIWI). (2020). *Principles and Practices of Integrated Water Resources Management. Retrieved from Manual1_final.* Stockholm International Water Institute. https://siwi.org/wp-content/uploads/2020/06/IWRM_Manual1_final.pdf

A. Marni Sandid, M. Bassyouni, Driss Nehari, & Y. Elhenawy. (2021). Experimental and simulation study of multichannel air gap membrane distillation process with two types of solar collectors. *Energy Conversion and Management, 243*(0196-8904), 114431.

Abdellatif, W., & Abdel Kader, S. (2023). Integrated Water Resources Management (IWRM) Plan as a Tool to Achieve Sustainable Water Management: Applying on Fouka Basin. *MSA Engineering Journal, 2*(4), 28-45.

Abu-Zeid, M. A.-R., Bassyouni, M., Fouad, Y., Monica, T., Sandid, A. M., & & Elhenawy, Y. (2023). Experimental and Simulation Study of Solar-Powered Air-Gap Membrane Distillation Technology for Water Desalination. *Membranes, Vol. 13*(10), pp. 821.

Bartholomew, T. V., Dudchenko, A. V., Siefert, N. S., & & Mauter, M. S. (2020). Cost optimization of high recovery single stage gap membrane distillation. *Journal of Membrane Science, Vol. 611*, 118370.

Belessiotis, V., Kalogirou, S., & Delyannis, E. (2016). Desalination Methods and Technologies—Water and Energy. In V. K. Belessiotis, *Thermal Solar Desalination Methods and Systems* (pp. 1-19). Elsevier Ltd.

Bendevis, P., Karam, A., & Laleg, T. M. (2019). Optimal Model-Free Control of Solar Thermal Membrane Distillation System. *Computers & Chemical Engineering*, 106622.

Boubakri, A., Elgharbi, S., & Bouguecha, S. -T. (2020). , & Hafiane, A. Energetic Performance and Permeate Flux Investigation of Direct-Contact Membrane Distillation for Seawater Desalination. *Chemical Engineering & Technology, 43*((12)), 2457–2468.

Boukhriss, M., Hamida, M.B.B., Maatoug, M.A, Zarzoum, K., Marzouki, R., & & Bacha, H. B. (2020). Correction to: The design of a unit sweeping gas membrane distillation: experimental study on a membrane and operating parameters. *Applied Water Science, 10*(7).

Boukhriss, M., Khemili, S., Ben Hamida, M.B, & Ben Bacha, H. (2018). Simulation and experimental study of an AGMD membrane distillation pilot for the desalination of seawater or brackish water with zero liquid discharged. *Heat Mass Transfer, 54*, 3521–3531.

Boukhriss, M., Maatoug, A., & Timoumi, M. (2021). Experimental investigation of a membrane distillation unit coupled with solar energy. In *Recent Advances in Environmental Science from the Euro-Mediterranean and Surrounding Regions (3rd Edition)* (Chapter 14). In R. Boukherroub, E. Lichtfouse, N. S. Tabrizi, & M. Gracia-Pinilla (Eds.): Springer, Cham.

Duong, , H. C., Cooper , P., Nelemans, B., Cath, Y. T., & Nghiem , D. L. (2016). Evaluating energy consumption of air gap membrane distillation for seawater desalination at pilot scale level. *Separation and Purification Technology, 166*, 55–62.

El Mokhtar, I., Boubakri, A., Bouguecha, S. A. T., & Hafiane, A. (2019). Modeling and experimental study of air gap membrane distillation unit: Application for seawater desalination. *Desalination and Water Treatment, 154*, 72–81.

Kabeel , A. E., Harby, K., Abdelgaied, M., & Eisa, A. (2019). A Comprehensive Review of Tubular Solar Still Designs, Performance, and Economic Analysis. *Journal of Cleaner Production*, 119030.

Karanasiou, A., Kostoglou, M., & & Karabelas, A. (2018). An Experimental and Theoretical Study on Separations by Vacuum Membrane Distillation Employing Hollow-Fiber Modules. *Water, Vol. 10*(7), pp. 947.

L. X., Hasson, D., Semiat, R., & Shemer, H. (2019). Intermediate concentrate demineralization techniques for enhanced brackish water reverse osmosis water recovery – A review. *Desalination, 466*, 24–35.

Mohamed H Koura, M. G. Mousa, Mohamed Khairat Dawood , & Tamer Nabil . (2025). Energy Management of Air Gap Membrane Distillation Unit. *Suez Canal Engineering, Energy and Environmental Science Journal*.

Mouche, M., Kebir, M., Mibarki, N., Triki, Z., Belhadj, A.-E., Tahraoui, H. Z., Amrane, A., Zhang, J., & & Mouni, L. (2023). An Effective Standalone Solar Air Gap Membrane Distillation Plant for Saline Water Desalination: Mathematical Model, Optimization. *Water, 15*(6), 1141.

Nakoa, K., Rahaoui, K., Date, A., & Akbarzadeh, , A. (2015). An experimental review on coupling of solar pond with membrane distillation. *Solar Energy, 119*, 319–331.

Perves Bappy, M. J., & Bahar, R. (2022). Improved production from an air gap membrane distillation desalination system. *Desalination and Water Treatment, 280*(1944-3986), 32-43.

Qasim, M., Samad, I. U., Darwish, N. A., & & Hilal, N. (2021). Comprehensive review of membrane design and synthesis for membrane distillation. *Desalination, Vol. 518*, pp. 115168.

Shahroie, B., Rajabi, L., & Derakhshan, A. A. (2016, , , (). . , 3(2)). Short review on membrane distillation techniques for removal of dissolved ammonia. *Journal of Applied Research in Water and Wastewater, 3*(2), 277-280.

Tai Z. S., Othman M. H. D., Koo K. N., & Jaafar J. (2023). Critical review on membrane designs for enhanced flux performance in membrane distillation. *Desalination, 553*(0011-9164), 116484.

Thakur, A. K., Hsieh, I.-M, Islam, M. R., Lin, B., Chen, C.-C., & & Malmali, M. (2020). Performance of sweeping gas membrane distillation for treating produced water: Modeling and experiments. *Desalination, Vol. 492*, pp. 114597.

The Open University. (2016). *open learn create*. www.open.edu. https://www.open.edu/openlearncreate/mod/oucontent/view.php?id=79936&section=4

Tijing, L. D., Woo, Y. C., Choi, J. S., Lee, S., Kim, S. H., & & Shon, H. K. (2015). Fouling and its control in membrane distillation—A review. *J. Membrane. Science, Vol. 475*, pp. 215–244.

U.S. Geological. (2023). *https://www.usgs.gov/special-topics/water-science-school/science/where-earths-water*. https://www.usgs.gov.

Viwanathan S., Reddy B. Sai. M., & Subbiah S. (n.d.). A 1-D model for hollow fiber vacuum membrane distillation: Performance and design analysis. *Journal of Water Process Engineering, 70*(2214-7144), 106984.

Z. Zhang, A.A. Atia, J.A. Andrés-Mañas, G. Zaragoza, & V. Fthenakis. (2022). Comparative techno-economic assessment of osmotically-assisted reverse osmosis and batch-operated vacuum-air-gap membrane distillation for high-salinity water desalination. *Desalination, 532*(0011-9164), 115737.

Zhou, Y., Chen, L., Huang, M., Hu, W., Chen, G., & & Wu, B. (2023). Experimental Investigation of the Desalination Process for Direct Contact Membrane Distillation Using Plate and Frame Membrane Module. *Applied Sciences, 13*(16), 9439.